2011

Boiling Heat Transfer and Flow Regimes in Microchannels – a Comprehensive Understanding

T. Harirchian
Purdue University

S V. Garimella
Purdue University, sureshg@purdue.edu

Harirchian, T. and Garimella, S V., "Boiling Heat Transfer and Flow Regimes in Microchannels – a Comprehensive Understanding" (2011). *CTRC Research Publications.* Paper 240.
http://dx.doi.org/10.1115/1.4002721

Boiling Heat Transfer and Flow Regimes in Microchannels—A Comprehensive Understanding[1]

Tannaz Harirchian

Suresh V. Garimella[2]
e-mail: sureshg@purdue.edu

School of Mechanical Engineering and Birck Nanotechnology Center,
Purdue University,
585 Purdue Mall,
West Lafayette, IN 47907-2088

Flow boiling in microchannels has been investigated extensively over the past decade for electronics cooling applications; however, the implementation of microchannel heat sinks operating in the two-phase regime in practical applications has lagged due to the complexity of boiling phenomena at the microscale. This has led to difficulties in predicting the heat transfer rates that can be achieved as a function of the governing parameters. From extensive experimental work and analysis performed in recent years, a clear picture has emerged that promises to enable prediction of flow boiling heat transfer over a wide parameter space. Experiments have been conducted to determine the effects of important geometric parameters such as channel width, depth, and cross-sectional area, operating conditions such as mass flux, heat flux, and vapor quality, as well as fluid properties, on flow regimes, heat transfer coefficients, and pressure drops in microchannels. A detailed mapping of flow regimes occurring under different conditions has been facilitated with high-speed flow visualizations. In addition, quantitative criteria for the transition between macro- and microscale boiling behaviors have been identified. In this paper, these recent advances toward a comprehensive understanding of flow boiling in microchannels are summarized. [DOI: 10.1115/1.4002721]

Keywords: microchannel flow boiling, confinement effects, microchannel dimensions, flow regime map, transition criteria

1 Introduction

Boiling in microchannels and minichannels has received much attention in recent years. Flow boiling regimes have been visualized and heat transfer rates and pressure drops compared with those in larger-scale channels. Two-phase flow under adiabatic conditions has also been studied. Garimella and Sobhan [1] pointed out that most of the literature on boiling in microchannels was targeted at electronics cooling applications and was focused on assessing and correlating the heat transfer coefficient, pressure drop, and critical heat flux; however, comprehensive predictive correlations or design guidelines for microchannels in two-phase operation are still unavailable. While the dependence of flow characteristics and heat transfer on channel geometry, operating conditions, and fluid properties has been investigated in a number of studies, only limited success has been achieved in generalizing results from specific studies to a wide range of microchannel parameters, as demonstrated quantitatively in Ref. [2]. In a recent review of flow boiling in small channels by Bertsch et al. [3], many conflicting trends were observed for dependence of boiling heat transfer on geometrical and flow parameters. Garimella and Sobhan [1] noted similar discrepancies between the results from various single-phase microchannel studies in the literature and related these conflicting trends to entrance and exit effects, nonuniformity of channel dimensions and differences in surface roughness, thermophysical property variations, nature of the thermal and flow boundary conditions, and uncertainties and errors in instrumentation, measurement, and measurement locations. These reviews demonstrate the clear need for systematic studies that carefully consider different parameters influencing transport in microchannels since a reliable prediction of the heat transfer rates and pressure drops in microchannels is not possible for design applications such as microchannel heat sinks due to the diversity in the results in the literature.

A review of the literature shows that the influence of a number of the governing parameters, such as microchannel geometry, mass flux, heat flux, vapor quality, and fluid properties, on flow boiling heat transfer was not clearly elucidated. In addition, issues such as flow instability, flow reversal, and large pressure drops were considered as potential impediments to practical implementation. Also, despite the large number of empirical correlations proposed for the prediction of boiling heat transfer and pressure drop in microchannels, robust design criteria for microchannel heat sinks are as yet unavailable due to the applicability of these correlations being limited to narrow ranges of experimental conditions [3,4].

Recent experimental investigations and analyses in the authors' group [3–17] have led to a more comprehensive understanding of the physical mechanisms and parameter dependencies in microchannel flow boiling, which promises to enable prediction of flow boiling heat transfer over a wide parameter space. The effects of important geometric parameters, operating conditions, and fluid properties on the flow regimes and thermal performance of microchannels have been determined through extensive experimental work. The present work summarizes these recent advances toward a comprehensive understanding of flow boiling in microchannels, along with detailed flow regime maps developed via high-speed flow visualizations, as well as quantitative criteria for the transition between macro- and microscale boiling behavior and nondimensional parameters that govern the occurrence and extent of flow confinement. Flow instability and flow reversal, as well as means for their mitigation, are also discussed.

2 Experiments

Several different substrates and fluids have been investigated in the experiments in the authors' group. The experiments conducted with a perfluorinated dielectric liquid, FC-77, using silicon test

[1]This manuscript is based on a keynote lecture delivered at THERMINIC, Leuven, Belgium, October 7–9, 2009.

[2]Corresponding author.

Contributed by the Electronic and Photonic Packaging Division of ASME for publication in the JOURNAL OF ELECTRONIC PACKAGING. Manuscript received January 24, 2010; final manuscript received May 17, 2010; published online March 2, 2011. Assoc. Editor: Tim Persoons.

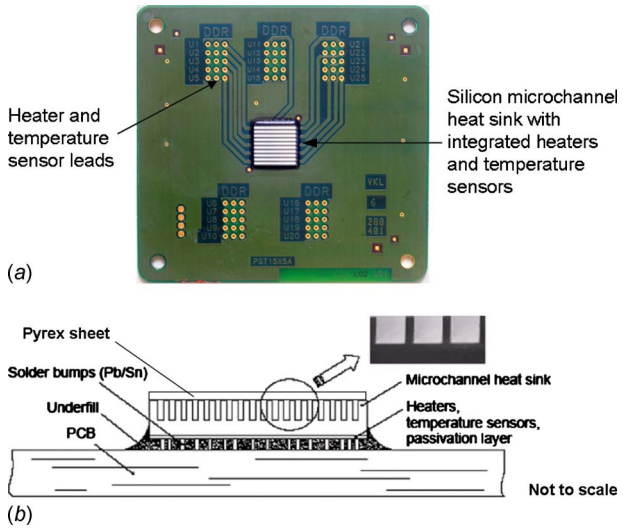

Fig. 1 (*a*) A representative microchannel test chip and (*b*) a schematic of the test chip cross section with integrated heaters and temperature sensors [11]

pieces with imbedded microscale temperature sensors are described here; other test facilities utilizing copper substrates and water and refrigerants as the working fluid are described in Refs. [5,6,8]. The silicon test pieces are used to study flow patterns, local heat transfer coefficients, and pressure drop during flow boiling in microchannels over a wide range of flow and geometric parameters. Only key features of the experiments are explained here; more details of the test section assembly, flow loop, and calibration procedures are available in Bertsch et al. [5].

2.1 Experimental Setup. The test loop consists of a magnetically coupled gear pump, a pre-heater installed upstream of the test section to heat the coolant to the desired subcooling temperature, and a water-to-air heat exchanger located downstream of the test section to cool the fluid before it enters a reservoir. The liquid is fully degassed before initiating each test using two degassing ports and the expandable reservoir. Details of the expandable reservoir design and the degassing procedure are available in Chen and Garimella [10]. A flow meter with a measurement range of 20–200 ml/min monitors the flow rate through the loop, and five T-type thermocouples are utilized to measure the fluid temperature at different locations in the loop. The pressure in the outlet manifold of the test section is maintained at 1 atm. The pressure in the inlet manifold and the pressure drop across the microchannel array are measured using a pressure transducer and a differential pressure transducer, respectively.

The microchannel test piece shown in Fig. 1 consists of a 12.7×12.7 mm^2 silicon substrate mounted on a printed circuit board. Parallel microchannels of rectangular cross section are cut into the top surface of the silicon chip using a dicing saw. A polycarbonate top cover positioned above the test piece and sealed with an O-ring provides enclosed passages for the liquid through the microchannels.

Included in the experimental investigation are 12 test pieces with microchannel widths ranging from 100 μm to 5850 μm and depths ranging from 100 μm to 400 μm. The aspect ratio and hydraulic diameter of the microchannels in the different test pieces take values from 0.27 to 15.55 and 96 μm to 707 μm, respectively. The width (w), depth (d), and number (N), along with the hydraulic diameter (D_h), aspect ratio (w/d), and single channel cross-sectional area (A_{cs}), of the microchannels in each test piece are provided in Table 1. The average roughness of the bottom wall of the microchannels ranges from 0.8 μm to 1.4 μm for the different test pieces, as measured by an optical profilometer; the bottom wall of the 100-μm-wide microchannels has a lower average roughness of 0.1 μm since a single dicing cut was used in their fabrication. The surface roughness of microchannel side walls is 0.1 μm, as measured by a probe-type profilometer.

A 5×5 array of individually addressable resistance heat sources is fabricated on the underside of the silicon chip. In the present work, a uniform heat flux is provided to the base of the microchannels. Also, a like array of temperature-sensing diodes facilitates local measurements of the base temperature. For a given current passing through a diode temperature sensor, the voltage drop across the diode determines the wall temperature. Details of the integrated resistance heaters and diode temperature sensors, as well as the procedures used to calibrate the heaters and sensors, are provided in Ref. [9].

Experiments are conducted with the 12 test pieces to study the effects of microchannel dimensions on the boiling heat transfer and flow patterns for four mass fluxes ranging from 225 kg/m^2 s to 1420 kg/m^2 s. For each test, the liquid is driven into the loop at a constant flow rate and is preheated to approximately 92°C, providing 5°C of subcooling at the inlet of the channels. While the flow rate and the inlet fluid temperature are kept constant throughout the test, the uniform heat flux provided to the chip is incremented from zero to the point at which the maximum wall temperature reaches 150°C, which is the upper limit for the safe operation of the test chips. Heat flux values approaching critical heat flux are not used in the experiments since the corresponding temperatures could cause the solder bumps in the test chip to fail.

At each heat flux and after the system reaches a steady state, high-speed visualizations are performed simultaneously with the heat transfer and pressure drop measurements. Movies of the flow

Table 1 Microchannel dimensions (the microchannel widths and depths are referred to in the rest of this paper by the nominal values that are provided) [11]

w nominal (actual) values (μm)	d nominal (actual) values (μm)	N	D_h (μm)	w/d	A_{cs} (mm^2)	η_o (%)
100 (99)	100 (94)	61	96	1.05	0.009	96.7–98.0
100 (97)	220 (217)	63	134	0.45	0.021	97.7–98.5
100 (102)	400 (369)	60	159	0.27	0.037	97.2–98.8
250 (240)	400 (371)	35	291	0.64	0.089	97.3–99.1
400 (398)	100 (65)	25	111	6.12	0.026	97.4–98.4
400 (400)	220 (197)	25	264	2.03	0.079	96.5–98.5
400 (395)	400 (365)	24	379	1.08	0.144	97.5–99.0
700 (686)	400 (376)	14	486	1.83	0.258	98.5–99.6
1000 (1024)	220 (226)	10	370	4.53	0.231	96.0–99.0
1000 (978)	400 (374)	10	541	2.62	0.366	99.2–99.7
2200 (2203)	400 (370)	5	634	5.95	0.815	99.6–99.9
5850 (5851)	400 (376)	2	707	15.55	2.201	99.8–99.9

patterns are captured at various frame rates ranging from 2000 fps to 24,000 fps, with the higher frame rates used for the smaller microchannels at the larger heat and mass fluxes. The images obtained from the camera are then post-processed using a MATLAB [18] code developed in-house to enhance the quality of the images, especially for those captured at higher frame rates.

2.2 Flow Instabilities. Chen and Garimella [10] investigated the effect of dissolved air on flow boiling of FC-77 in microchannels using a carefully designed degassing scheme. Their study showed that dissolved air significantly affects both heat transfer and pressure drop in microchannels. For gassed liquid, boiling incipience temperatures are lower than the saturation values, resulting in an earlier incipience of boiling and, subsequently, an earlier increase in heat transfer coefficient; however, at high heat fluxes, the heat transfer coefficients for degassed and gassed liquid reach similar values. The pressure drops were shown to be larger for the gassed liquid. Also, larger flow instabilities in terms of pressure drop fluctuations were observed for the gassed liquid and an increase in flow instabilities was detected with increasing heat flux.

In all the rest of the experiments conducted in the authors' group, the liquid in the test loop is fully degassed before initiating each test to help minimize flow instabilities. Also, a throttling valve positioned upstream of the test section serves to suppress instabilities in the microchannel heat sink. Mild flow reversals were still observed at the inlet of the microchannels at the highest heat fluxes studied for microchannels of cross-sectional area of 0.144 mm^2 and smaller. However, these instabilities did not affect the inlet fluid temperature, which is held constant throughout each test. Also, repeatability of the experiments was confirmed [19], and it is illustrated that maintaining the same operating conditions, very similar heat transfer and pressure drop data are obtainable from different tests.

2.3 Data Reduction. The local heat transfer coefficient, h, is calculated from

$$h = q_w'' / \eta_o (T_w - T_{\text{ref}}) \tag{1}$$

where T_{ref} is the local mean fluid temperature in the single-phase region and the liquid saturation temperature in the two-phase region and T_w is the local microchannel wall temperature. $\eta_o = 1 - NA_f/A_t(1-\eta_f)$ is the overall surface efficiency of the microchannel heat sink and is listed in Table 1 for all microchannels considered. The heat flux used in Eq. (1) is the wall heat flux and is defined as

$$q_w'' = \dot{q}_{\text{net}}/(A_t/25) \tag{2}$$

where $\dot{q}_{\text{net}}$ is the net heat transfer rate to the fluid and A_t is the total heated area of the microchannels, with L being the microchannel length:

$$A_t = N(w + 2d)L \tag{3}$$

The calculated local heat transfer coefficients presented here are based on measurements from the temperature sensor located along the centerline of the test piece near the flow exit. Flow visualizations are also reported for this location. More information on the data reduction can be found in Ref. [9].

Important nondimensional parameters often used in flow boiling include Reynolds number, Re, Bond number, Bo, and boiling number, Bl. Reynolds number is calculated using the liquid phase mass flux as

$$\text{Re} = GD/\mu \tag{4}$$

where G is the liquid mass flux and μ is the dynamic viscosity of the liquid. Bond number represents the ratio of buoyancy force to surface tension force and assumes importance in microscale boiling:

$$\text{Bo} = g(\rho_f - \rho_g)D^2/\sigma \tag{5}$$

Here, ρ_f and ρ_g are the density of the liquid and vapor phases, respectively, and σ is the liquid surface tension.

As demonstrated in Harirchian and Garimella [11], the channel's cross-sectional area plays a critical role in determining microchannel boiling mechanisms and heat transfer; therefore, the length scale used in Eqs. (4) and (5) is the square root of the cross-sectional area of one channel rather than its hydraulic diameter. Boiling number is the nondimensional form of the heat flux and is calculated using the liquid mass flux and latent heat, h_{fg}, as follows:

$$\text{Bl} = q_w''/(Gh_{fg}) \tag{6}$$

Following a standard uncertainty analysis [20], the uncertainties associated with the wall heat flux and the heat transfer coefficient are estimated to be 2% to 4% and 2.2% to 4.8%, respectively, for the cases considered. Details of the measurement uncertainties are discussed in Ref. [11].

3 Results and Discussion

3.1 Flow Regimes. In Harirchian and Garimella [12], flow visualizations were performed with simultaneous heat transfer measurements during flow boiling in microchannels of different sizes for different flow rates. Five major flow regimes of bubbly, slug, churn, wispy-annular, and annular flow and a post-dryout regime of inverted-annular flow were identified in these microchannels, for which representative visualization images are provided in Fig. 2. Detailed descriptions of these regimes and the changes in flow regimes with microchannel size and mass flux are discussed in detail in Ref. [12].

Figure 3 shows a summary of the existing flow regimes at different microchannel sizes and mass fluxes. It is seen that in the smaller microchannels and at lower mass fluxes, bubbly flow is not established; instead, slug flow is observed for low heat fluxes. In slug flow, elongated vapor bubbles are confined within the channel's cross section and are separated from the walls by a thin liquid layer. As the heat flux is increased, an alternating churn and confined annular flow appears in these microchannels. In confined annular flow, the vapor core occupies the whole cross section of the microchannels and is separated from the walls by a thin liquid film.

As the channel's cross-sectional area or the mass flux increases, bubbly flow is observed at low heat fluxes. In the bubbly flow regime, bubbles are smaller relative to the cross section of the channels and confinement is not observed. At higher heat fluxes, alternating churn and wispy-annular or annular flow occurs. In wispy-annular or annular flow, the vapor core does not necessarily occupy the entire cross section and can instead exist on only one side of the channel; in other words, the flow is not confined by the channel walls. For example, as can be seen in Fig. 4(*b*) for the 2200×400 μm^2 microchannels, the wispy-annular flow (or annular flow in Fig. 4(*c*)) and churn flow patterns are distributed side by side across the width of the channel due to the large channel aspect ratio, as also explained in Ref. [12].

Another geometric parameter that affects flow boiling is surface topography. Jones et al. [13] investigated the effects of surface roughness on flow regimes and heat transfer characteristics in pool boiling of water and FC-77. Their experiments showed that at low heat fluxes, more activation sites were observed for roughened surfaces (roughness average of 5.89 μm) relative to the polished surfaces (roughness average of 0.04 μm). Also, rougher surfaces led to smaller bubble departure diameter and higher bubble emission frequency.

3.2 Microscale Phenomena and Vapor Confinement. There has been a good deal of discussion in the literature regarding the appropriate definition of a microchannel; however, a clear, physics-based distinction of microchannels from conventional-

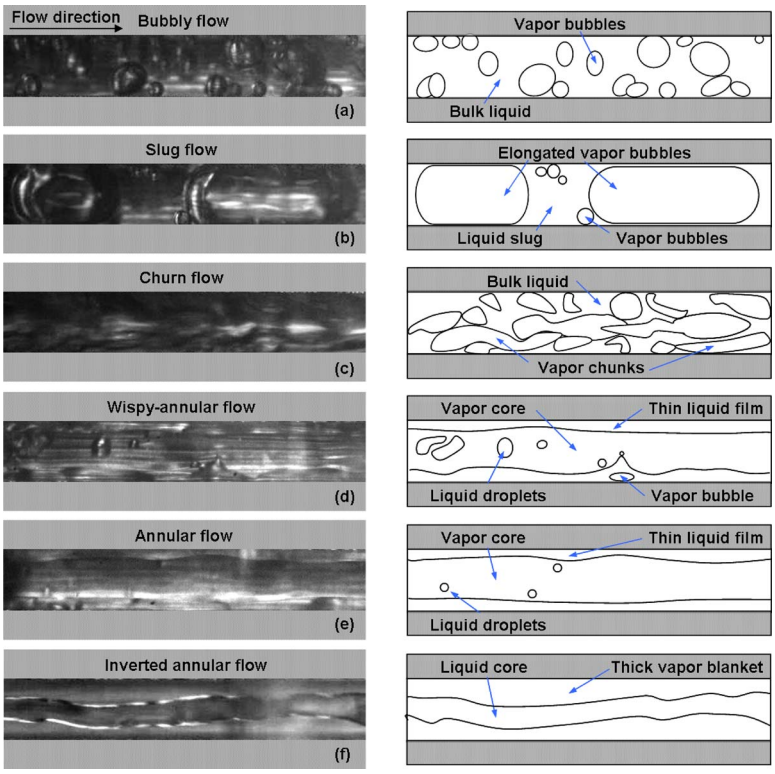

Fig. 2 Description of observed flow boiling regimes [12]

sized channels has not emerged. In general, a microchannel refers to a channel for which the heat transfer coefficient and pressure drop deviate from the predictions from widely accepted models for conventional-sized channels. For single-phase flow, Liu and Garimella [21] and Lee et al. [22] showed that channels with hydraulic diameters as small as 244 μm (the minimum considered in the studies) still exhibit heat transfer and pressure drop behavior that is well-predicted by conventional models. With boiling present in the channels, however, the flow phenomena differ from those in macroscale channels as the channel approaches the bubble diameter in size. In these small channels, correlations and models developed for larger channels no longer apply [3]. Harirchian and Garimella [14] developed a new criterion for delineating microchannels from macroscale channels based on the presence of vapor confinement, as explained below.

The experimental flow visualizations [11,12] reveal that the flow confinement depends not only on the channel size but also on the mass flux since the bubble diameter varies with flow rate. The different experiments carried out for various channel sizes and mass fluxes in Refs. [11,12] can be categorized into two groups of confined and unconfined flow regardless of the heat input and are represented in Fig. 5 on Reynolds number and Bond number coordinates. This plot shows that for channels of small cross-sectional area and at low mass fluxes, vapor confinement is observed, while for larger microchannels and at high mass fluxes, the flow is not confined. The solid line on this plot shows the transition between confined and unconfined flow and is a curve fit to the transition points represented by

$$\mathrm{Bo}^{0.5} \times \mathrm{Re} = \frac{1}{\mu}\left[\frac{g(\rho_f - \rho_g)}{\sigma}\right]^{0.5} GD^2 = 160 \qquad (7)$$

$\mathrm{Bo}^{0.5} \times \mathrm{Re}$, a parameter termed as the *convective confinement number* here, is proportional to the mass flux, G, and the cross-sectional area, D^2, and is inversely proportional to the fluid surface tension. This new flow boiling transition criterion recommends that for $\mathrm{Bo}^{0.5} \times \mathrm{Re} < 160$, vapor bubbles are confined and the channel should be considered as a microchannel. For larger convective confinement numbers, the flow does not experience physical confinement by the channel walls and the channel can be considered as a conventional (macroscale) channel. It is important to note that this transition criterion is independent of the heat flux and is very useful in determining whether a channel behaves as a microchannel or a conventional, macroscale channel, regardless of the heat input, for practical applications. A comprehensive flow regime map accounting for the heat input that determines the specific flow patterns is presented in Sec. 3.7.

In Harirchian and Garimella [14], the proposed criterion for transition between confined and unconfined flow is compared with available experimental observations from other studies in the literature for water and fluorocarbon liquids. The comparison shows that the proposed criterion is successful in predicting the confined or unconfined nature of the flow from a variety of studies in the literature.

The effects of the physical confinement by the channel walls on the heat transfer coefficient and boiling curves are discussed next.

3.3 Heat Transfer Coefficients and Boiling Curves. Heat transfer coefficients and boiling curves have been studied extensively by the authors' group and the effects of several geometric and flow parameters on flow boiling heat transfer have been systematically investigated [4–17,23,24], as summarized in Secs. 3.3 and 3.4.

Figure 6 illustrates the effect of microchannel dimensions on the heat transfer coefficient for a fixed mass flux of 630 $\mathrm{kg/m^2\,s}$ [11]. In this figure, the heat transfer coefficient is plotted versus the wall heat flux for both single-phase and two-phase flows in all the microchannels considered. As can be seen from this figure, the onset of boiling is associated with an increase in the wall heat transfer coefficient.

A careful examination of this figure reveals that at this mass flux, for microchannels with a cross-sectional area of 0.089 $\mathrm{mm^2}$ and larger, the heat transfer coefficient is independent of micro-

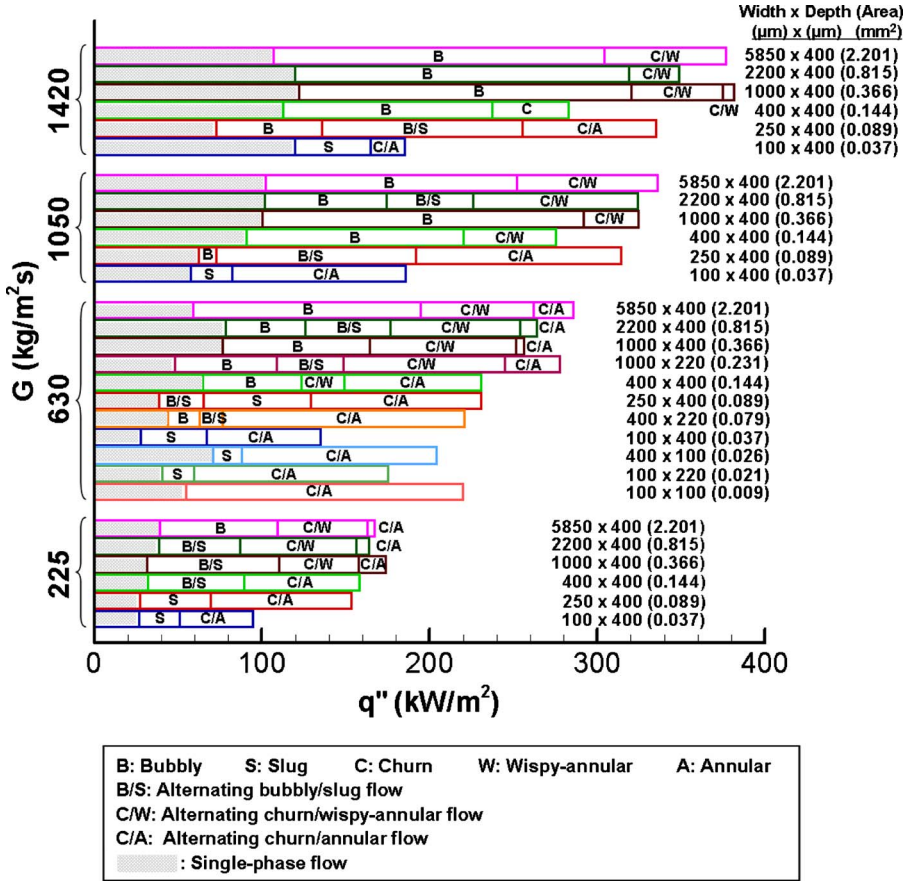

Fig. 3 Summary of boiling flow patterns in the microchannel test pieces; the microchannel dimensions are presented as width (μm)×depth (μm) with a single-channel cross-sectional area (mm²) in parentheses [14]

channel size. For smaller cross-sectional areas where bubble confinement was visually observed, the heat transfer coefficient behavior is markedly different, with the heat transfer coefficient being relatively higher at the lower heat fluxes. As the heat flux increases, the curves cross over, resulting in lower values of heat transfer coefficient. The largest heat transfer coefficient is seen in the 100×220 μm^2 microchannels, with a cross-sectional area of 0.021 mm^2, before partial dryout occurs. For the 100×100 μm^2 microchannels, the heat transfer coefficient is relatively lower at low heat fluxes since partial dryout occurs even at very low heat fluxes.

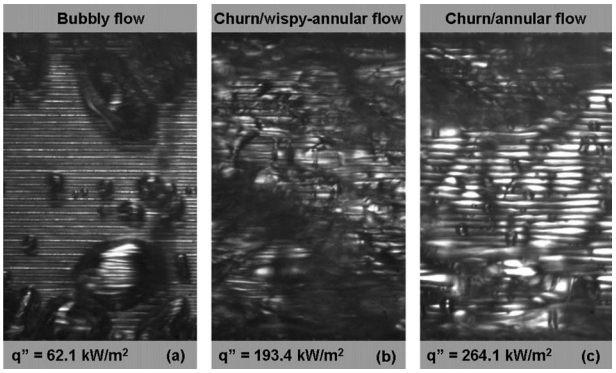

Fig. 4 Flow patterns in the 2200×400 μm^2 microchannels at the three different heat fluxes; G=630 kg/m² s [11]

The larger heat transfer coefficients in the smaller microchannels are attributed to the confinement effects caused by bubbles occupying the whole cross section of the microchannels due to the small cross-sectional area relative to the bubble diameter at departure. As discussed in Secs. 3.1 and 3.2 above, flow visualizations reveal that in all of the microchannels with cross-sectional area

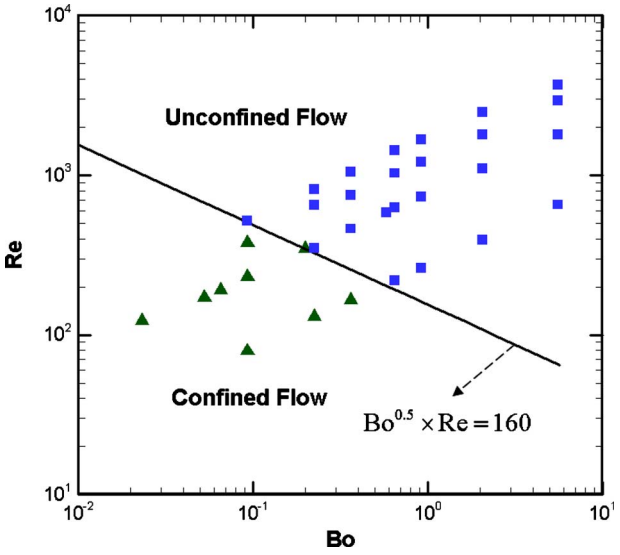

Fig. 5 Transition from confined flow to unconfined flow [14]

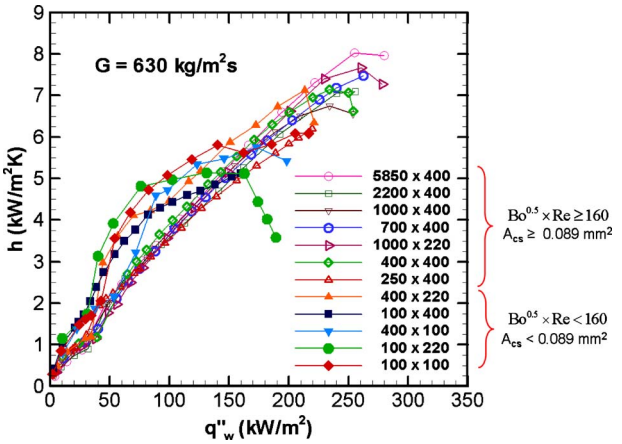

Fig. 6 Effect of microchannel dimensions (width (μm) $\times$depth (μm)) on heat transfer coefficients [11]

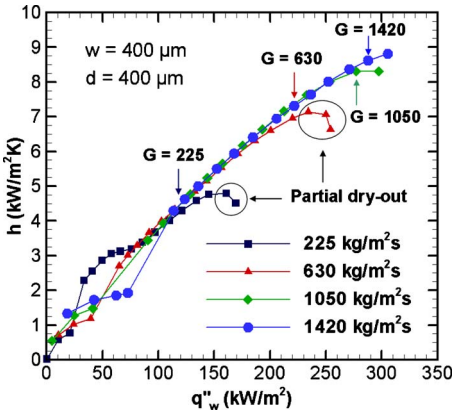

Fig. 7 Effect of mass flux on heat transfer coefficients; the arrows mark the heat fluxes at which suppression of nucleate boiling is observed [12]

and mass flux values leading to a convective confinement number less than 160, slug flow commences soon after incipience of boiling and flow enters the churn/annular regime at relatively low heat fluxes. Early establishment of annular flow in microchannels of very small diameter was also reported in other studies [25,26]. As a result, bubble nucleation at the walls is not the only heat transfer mechanism, and the evaporation of the thin liquid film at the walls in the slug and annular flows also contributes to the heat transfer. Therefore, the value of heat transfer coefficient is larger for these smaller microchannels at lower heat fluxes. At high heat fluxes, a decrease in heat transfer coefficient is detected, which is due to an early partial wall dryout in these small channels. In microchannels with larger cross-sectional areas, nucleate boiling is the dominant flow regime, and hence, the heat transfer coefficient is independent of channel size. Similar trends have been reported in the literature for the dependence of confined pool boiling on plate spacing in parallel-plate configurations; as the plate spacing was reduced below the bubble departure diameter, heat transfer was enhanced in the low heat flux region due to confinement effects. As the spacing was decreased further, the heat transfer coefficient increased until it reached a maximum, after which, it deteriorated with decreasing channel spacing [27].

It is emphasized that it is neither the channel's aspect ratio nor the smallest dimension of the microchannel that is the determining geometric dimension affecting boiling heat transfer but instead, the channel's cross-sectional area [11].

Similar plots for three other mass fluxes are shown in Ref. [14]. These plots showed that for the channels in which confinement is not present and nucleate boiling is dominant up to very high heat fluxes and for which the convective confinement number $Bo^{0.5} \times Re$ is larger than 160, the heat transfer coefficient is independent of microchannel size; all the curves collapse on to a single curve in these cases. For microchannel dimensions and mass fluxes that result in $Bo^{0.5} \times Re < 160$, the heat transfer coefficients are larger due to the contribution of thin-film evaporation to the heat transfer mechanisms.

The effect of mass flux on heat transfer coefficient was investigated in Harirchian and Garimella [9]. In Fig. 7, heat transfer coefficients are plotted as a function of the wall heat flux for different mass fluxes. The heat transfer coefficient increases with mass flux in the single-phase region for a fixed wall heat flux. After the onset of nucleate boiling, however, the heat transfer coefficient becomes independent of mass flux and increases with heat flux. At high levels of wall heat flux, as the contribution from convective heat transfer begins to dominate that of nucleate boiling, the heat transfer coefficient becomes a function of mass flux and increases with increasing mass flux. Flow visualizations performed for these cases show that the plots of heat transfer coefficient diverge from each other at the heat flux where the bubble nucleation is suppressed at the walls. Other microchannel sizes tested yielded similar trends for the dependence of heat transfer coefficient on mass flux. These results regarding the dependence of heat transfer coefficient on flow rate are also consistent with the findings of Chen and Garimella [15,16].

At high heat fluxes, a decrease in heat transfer coefficient is detected. Flow visualizations reveal that this is attributed to a partial wall dryout, as also reported in Ref. [15].

In Harirchian and Garimella [11], boiling curves are discussed for different channel sizes and a mass flux of 630 kg/m^2 s, as shown in Fig. 8. It is shown that for microchannels of cross-sectional area of 0.089 mm^2 and larger, the boiling curves cluster together beyond the onset of nucleate boiling, indicating the dominance of nucleate boiling. As boiling starts in these microchannels, the wall temperature shows a weak dependence on the heat flux. This is consistent with the dominant nucleate boiling flow regime that was observed through the flow visualizations. As the heat flux increases, the wall temperature becomes more dependent on the heat flux and the boiling curves deviate for different channel sizes as convective boiling dominates. For the microchannels with smaller cross-sectional areas, the wall temperature increases with increasing wall heat flux and the boiling curves deviate from those of the larger microchannels. The strong dependence of the wall temperature on the heat flux for these microchannels can be explained based on the flow visualizations, which reveal that thin-

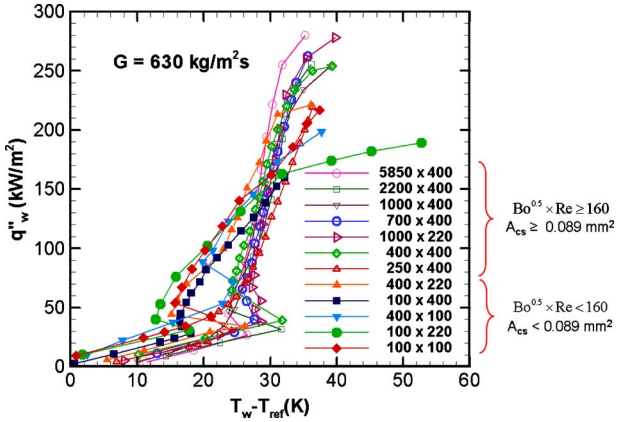

Fig. 8 Effect of microchannel dimensions (width (μm) $\times$depth (μm)) on boiling curves [11]

film evaporation and forced convection in the thin liquid film surrounding the vapor slug or annulus, rather than nucleate boiling, are the main heat transfer mechanisms in the smaller channels.

Harirchian and Garimella [9] also investigated the effect of mass flux on the boiling curves. It was shown that for cases later determined as having a convective confinement number of larger than 160, the boiling curves for all mass fluxes collapse to a single curve beyond the onset of nucleate boiling, indicating the dominance of nucleate boiling. For the mass fluxes at which confinement occurs, the boiling curves deviated from other curves due to an early transition to slug flow and annular flow regimes at lower and higher heat fluxes, respectively.

Holcomb et al. [23] investigated the influence of microchannel size and mass flux on flow boiling of deionized water in silicon microchannels. Their experiments were conducted over a similar range of parameters as in the FC-77 studies discussed thus far, and similar trends for dependence of heat transfer performance on channel dimensions and flow rate were observed; the boiling curves and heat transfer coefficients were found to be largely independent of channel size and mass flux, except in the vicinity of transition from single-phase to two-phase, indicating the dominance of nucleate boiling for the parameters considered.

The influence of surface roughness on flow boiling heat transfer has also been investigated with deionized water [17]. These experiments indicated only a small influence of surface roughness on boiling incipience and on saturated boiling heat transfer coefficients at low heat fluxes. At higher heat fluxes, however, a heat transfer enhancement of 20–35% was obtained with the rougher surfaces (roughness average of 3.9 μm and 6.7 μm) relative to the smooth surfaces (1.4 μm). The effect of surface roughness on pool boiling heat transfer was also studied by Jones et al. [13]. They observed a continuous increase in heat transfer coefficient with increasing surface roughness in pool boiling of FC-77; however, experiments with water showed little improvement in heat transfer with increasing surface roughness except for very rough surfaces with an average roughness of 10 μm at which a significant increase in heat transfer coefficient was observed. It should be noted that the test chips considered for flow boiling studies with FC-77 have smooth surfaces.

3.4 Effect of Vapor Quality. It is also important to understand the variation of flow boiling heat transfer coefficient as a function of vapor quality. Bertsch et al. [5,6] investigated flow boiling of refrigerant HFC-134a in parallel copper microchannels of dimensions 762×1905 μm^2 as a function of local vapor quality. A custom-designed experimental setup allowed for the measurement of heat transfer coefficients at specific vapor qualities spanning the entire range from subcooled liquid to superheated vapor. The heat transfer coefficient was found to vary significantly with vapor quality; it increased as the vapor quality was increased from subcooled liquid and reached a peak at a local vapor quality of 20%, after which it dropped again sharply for further increases in vapor quality.

In flow boiling of FC-77, the heat transfer coefficient increases with increasing exit vapor quality [24] until the point of partial dryout, whereupon a decrease in heat transfer coefficient is observed. It is also noted that larger exit qualities could be achieved in smaller microchannels under the same mass flux and heat flux conditions, resulting in early transition to annular flow and larger values of heat transfer coefficient in these smaller channels.

3.5 Pressure Drop. The pressure drop and pumping power is now considered, along with the influence of channel dimensions and mass flux on these quantities.

The pressure drop as a function of the average wall heat flux is shown in Fig. 9 for a wide range of microchannel sizes. The two-phase region can be clearly distinguished from the single-phase region by the sharp change in the slope of the curves. In the single-phase region, the pressure drop slightly decreases with increasing heat flux due to the reduction in liquid viscosity as the liquid temperature increases. In the two-phase region, the pressure drop is strongly dependent on heat flux and increases rapidly and almost linearly with increasing heat flux due to the acceleration of vapor, as also reported in other studies [15,28,29].

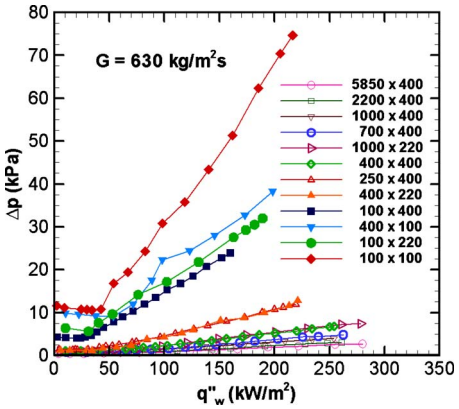

Fig. 9 Effect of microchannel dimensions (width (μm) $\times$ depth (μm)) on pressure drop [11]

In both the single-phase and two-phase regions, the pressure drop increases with decreasing microchannel cross-sectional area at a given heat flux. In the two-phase region, the slope of the line also increases as the channel area decreases, with much larger pressure drops for smaller channels at higher heat fluxes.

It is also seen that for the microchannels with similar cross-sectional areas and different aspect ratios (e.g., 250×400 μm^2 and 400×220 μm^2 microchannels), the pressure drops are similar in value.

For a fixed channel size, in both single-phase and two-phase regions, the pressure drop increases with increasing mass flux [9], which agrees with the results of Pate et al. [29]. Chen and Garimella [15], however, found that the pressure drop was independent of mass flux in the two-phase region. They attributed this observation to the balance between the frictional pressure drop and accelerational pressure drop under the moderate inlet subcooling considered in their tests, which is in contrast to the very modest subcooling used in the current work.

The experimental results for pressure drop have also been compared with predictions from several empirical correlations in the literature [30]. The comparisons reveal the failure of these correlations to provide a suitable prediction of the experimental results and the need for physics-based models for flow boiling in microchannels.

The pumping power required to manage a given base heat flux with different microchannel sizes is also of practical interest. In the single-phase region, the pumping power required is almost constant, independent of the heat flux, while in the two-phase region, the pumping power increases rapidly with heat flux [9]. The experiments reveal that for microchannels without vapor confinement, the pumping power is not a strong function of microchannel width. As the microchannel size decreases below the confinement threshold, however, the pumping power increases with decreasing channel size. Therefore, for a given pumping power, more heat can be removed from the heat source with larger microchannels.

3.6 Heat Transfer Predictions. A large number of correlations have been proposed in the literature for predicting heat transfer coefficients for pool boiling and flow boiling in tubes and channels. Of the many predictive correlations for boiling heat transfer, those of Cooper [31] and Gorenflo [32] are widely used for predicting nucleate pool boiling heat transfer coefficients. Flow boiling features simultaneous contributions from nucleate boiling and forced convection. There have been two main ap-

proaches to model flow boiling: a superposition approach and an extrapolation approach [7]. Chen [33] suggested the superposition approach in which the nucleate boiling and forced convection components are linearly summed with the introduction of a suppression factor for the nucleate boiling term and an enhancement factor for the forced convection term. Shah [34] proposed an extrapolation-type correlation that used a boiling number and a convective number. Following these two early studies, many modifications have been proposed to both approaches to obtain better agreement with different sets of experimental data for conventional channels [35,36]. In the past decade, experiments have focused on mini- and microchannels and the forced convection component in flow boiling correlations has been adapted for laminar or developing flows [28,32,37,38] to better represent the flow conditions in mini- and microchannels.

The experimental results obtained by the authors were compared with predictions for the same conditions from ten correlations from the literature in Harirchian and Garimella [9]. Both pool boiling and flow boiling correlations for both macro- and microchannels were considered. For most of the experimental cases (with $\mathrm{Bo}^{0.5} \times \mathrm{Re} > 160$), the nucleate pool boiling correlation of Cooper [31] predicted the experimental results very well with a mean absolute error of 7.2%. For smaller microchannels at lower mass fluxes (which would exhibit vapor confinement according to the criterion proposed here), the error associated with the prediction of heat transfer coefficient using this correlation was larger at 15%; however, this pool boiling correlation still predicted the experimental results better than other empirical correlations developed specifically for microchannel flow boiling.

In a recent review [3], 25 published heat transfer correlations were examined to identify the applicability of correlations developed both for conventional-sized and microscale channels in predicting the heat transfer coefficient in small channels; 1847 experimental data points were compiled from ten different published studies, which reported flow boiling heat transfer measurements in channels of hydraulic diameter less than 2 mm. Again, the pool boiling correlation of Cooper [31] showed the lowest deviation between experimental measurements and predictions, indicating the dominance of the nucleate boiling heat transfer regime. This study [3] showed that none of the correlations developed for flow boiling offered an improved prediction over pool boiling correlations. In particular, correlations developed especially for minichannels and microchannels show essentially no improvement over those developed earlier for conventional-sized channels. Summaries of all the correlations assessed, along with their conditions and ranges of applicability, are tabulated in Refs. [3,9].

Based on the clear need that was identified for flow boiling correlations that are applicable over a wide range of parameters, Bertsch et al. [4] developed a composite correlation that included both nucleate boiling and convective heat transfer terms while taking into account for the confinement in small channels. They compared their proposed correlation to 3899 data points from 14 studies in the literature for 12 fluids with a wide range of hydraulic diameters, confinement numbers, mass fluxes, heat fluxes, and vapor qualities and achieved a mean absolute error of less that 30%.

Subsequent experimental heat transfer measurements with water [23] obtained under the same conditions and parameters as those discussed here for FC-77 also compared well with predictions from the correlations of Cooper [31] and Bertsch et al. [4], with mean absolute errors of 23.2% and 24.6%, respectively.

This discussion of the literature and the comparison of experimental results from a wide range of experimental studies with existing empirical correlations point to a clear need for physics-based models for flow boiling heat transfer in microchannels. Such models should account for microscale effects and must be validated against a large experimental database, featuring a wide range of parameters and operating conditions. Flow regime maps must first be developed to determine the flow patterns present for any given set of parameters. Physics-based models for each of the flow regimes can then be developed and validated using such a database.

3.7 Flow Regime Maps. Flow regime maps are commonly used to determine the flow patterns that exist under different operating conditions, as well as the conditions for flow pattern transitions. Such maps are essential to the development of flow regime-based models for the prediction of the heat transfer rate and pressure drop in flow boiling. The coordinates used to plot these flow regime maps can be superficial phase velocities or derived parameters containing these velocities; however, the effects of important parameters such as channel size are not represented in a number of these maps. Early flow regime maps for horizontal and vertical two-phase flow in channels with diameters of a few centimeters were developed by Baker [39], Hewitt and Roberts [40], and Taitel and Dukler [41]. In recent years, a few studies [42–44] have developed flow regime maps for boiling in microchannels and have shown that flow regime maps developed for larger tubes are inapplicable for predicting flow regime transitions in microchannels. Flow regime maps for adiabatic two-phase flow in microchannels were also proposed through high-speed visualizations [45–47]; however, it has been shown [44] that adiabatic flow regime maps are not suitable for the prediction of microscale boiling. Despite the inability of macroscale boiling maps or adiabatic two-phase flow regime maps to predict the boiling flow patterns in microchannels, a review of the literature shows a dearth of investigations into flow regime maps specifically targeted at microchannels undergoing flow boiling that are applicable to a wide range of microchannel dimensions and experimental conditions.

In recent work by the authors [12], two different types of flow regime maps for microchannel flow boiling of FC-77 have been developed based on the experimentally visualized flow patterns. Twelve different flow regime maps were plotted for the six channel dimensions considered using coordinates of mass flux and vapor quality, and alternatively, of liquid superficial velocity and vapor superficial velocity. Both types of flow regime maps depend on channel dimensions; hence, for each channel dimension, a separate flow regime map is required to capture the flow regime transitions accurately. The effects of channel width on the flow regime transition were discussed as well. The flow regime maps developed in Ref. [12] were also compared with flow transitions from other studies in the literature for adiabatic two-phase flow and for boiling in macro- and microchannels. It was concluded that only the flow regime maps developed for microscale flow boiling in comparable channel sizes could reasonably match the observed flow transitions.

Due to dependence of flow regimes (and regime maps) on channel dimensions, it is important to include the effects of channel size in the flow regime maps. To address this need, a comprehensive flow regime map has recently been developed [14] and is discussed here.

Figure 10 shows the comprehensive flow regime map developed based on the experimental results and flow visualizations performed with FC-77. The abscissa in this plot is the newly defined convective confinement number, $\mathrm{Bo}^{0.5} \times \mathrm{Re}$, which is proportional to the dimensional quantity, $G \times D^2$. The ordinate, $\mathrm{Bl} \times \mathrm{Re}$, is a nondimensional form of the heat flux, which is proportional to $q''_w \times D$. Plotting all the ~390 experimental data points obtained in Refs. [11,12] for flow boiling of FC-77 in 12 different microchannel test pieces with channel cross-sectional area in the range of 0.009–2.201 mm^2, four mass fluxes in the range of 225–1420 $\mathrm{kg/m^2\,s}$ and heat fluxes in the range of 25 $\mathrm{kW/m^2}$ to 380 $\mathrm{kW/m^2}$ on $\mathrm{Bl} \times \mathrm{Re}$ versus $\mathrm{Bo}^{0.5} \times \mathrm{Re}$ logarithmic axes leads to a comprehensive flow regime map with four distinct regions of confined slug flow, churn/confined annular flow, bubbly flow, and churn/annular/wispy-annular flow.

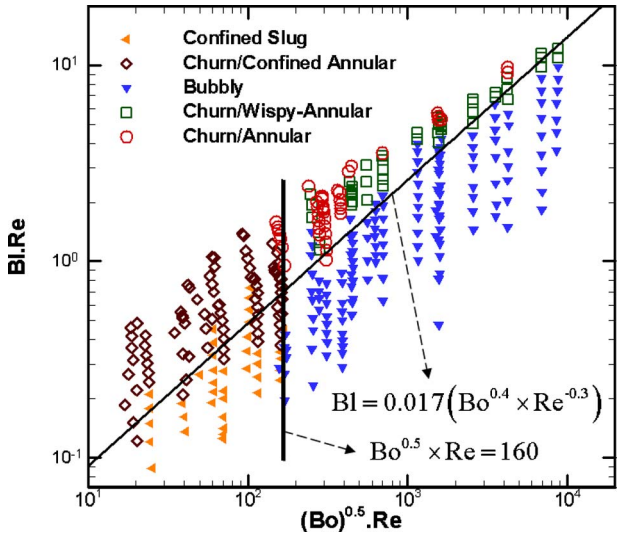

Fig. 10 Comprehensive flow regime map, including regime transitions, for FC-77 [14]

The vertical transition line is given by $Bo^{0.5} \times Re = 160$, which represents the transition to confined flow. The other transition line is a curve fit to the points of transition from bubbly or slug flow to alternating churn/annular or churn/wispy-annular flow and is given by

$$Bl \times Re = 0.017(Bo^{0.5} \times Re)^{0.7} \quad (8)$$

which can be rearranged to give

$$Bl = 0.017(Bo^{0.4} \times Re^{-0.3}) \quad (9)$$

This flow regime map shows that for $Bo^{0.5} \times Re < 160$, vapor confinement is observed in both slug and churn/annular flow regimes, while for $Bo^{0.5} \times Re > 160$, the flow is not confined. For low heat fluxes with $Bl < 0.017(Bo^{0.4} \times Re^{-0.3})$, flow patterns of slug (if $Bo^{0.5} \times Re < 160$), or bubbly (if $Bo^{0.5} \times Re > 160$) flow exist in the microchannels. At higher heat fluxes with $Bl > 0.017(Bo^{0.4} \times Re^{-0.3})$, vapor bubbles coalesce, resulting in a continuous vapor core in the alternating churn/annular or churn/wispy annular flow regimes.

In Ref. [14], experimental data from a range of other studies in the literature were plotted on this comprehensive flow regime map. The map developed was clearly able to represent the flow regimes found in the literature for water and fluorocarbon liquids.

4 Conclusion

Extensive experimental work has been conducted with microchannel test pieces encompassing a wide range of channel dimensions over a broad range of operating conditions to systematically determine the effects of important geometric and flow parameters on flow regimes, heat transfer, and pressure drop associated with microscale flow boiling. Local heat transfer measurements obtained with simultaneous, detailed flow visualizations have led to a better understanding of boiling phenomena in microchannels and the governing heat transfer mechanisms. The extensive microscale boiling experiments and analyses have resulted in a comprehensive understanding of boiling, with some of the significant findings listed below:

- A large database of boiling flow pattern visualizations is obtained for a wide range of channel dimensions and flow parameters, leading to a good understanding of microscale flow regimes.
- A clear knowledge of the effects of microchannel dimensions on flow boiling is obtained; the cross-sectional area of the microchannels is found to play a determining role in boiling mechanisms and heat transfer.
- Vapor confinement and emergence of microscale effects are shown to depend not only on channel size and fluid properties but also on the flow rate. Based on the experimental results, a new transition criterion is developed that predicts the conditions under which microscale confinement effects are exhibited in flow boiling.
- For conditions under which flow confinement does not occur, the heat transfer and boiling curves are independent of channel size and flow rate and pressure drop and pumping power have only minor sensitivity to channel size and flow rate.
- In confined flow, the heat transfer coefficient increases as the cross-sectional area of the microchannels decreases. Thin liquid film evaporation in confined boiling results in larger values of heat transfer coefficients relative to unconfined flow where nucleate boiling is dominant.
- Effects of surface roughness on pool boiling and flow boiling have been studied for water and dielectric liquids; surface roughness is found to have a minor effect on heat transfer coefficient at low heat fluxes while it leads to a 20–35% enhancement at higher heat flux region in flow boiling of water.
- Empirical correlations are developed for prediction of heat transfer coefficient based on a large data set of approximately 3900 data points from several studies in the literature.
- A comprehensive flow regime map for flow boiling of FC-77 is developed, along with quantitative regime transition criteria, based on approximately 390 data points encompassing a wide range of microchannel dimensions, mass fluxes, and heat fluxes. This comprehensive flow map is expected to facilitate the development of flow regime-based models for the prediction of boiling heat transfer coefficients.

Acknowledgment

Financial support from the State of Indiana 21st century research and technology fund and from the Cooling Technologies Research Center, a NSF Industry/University Cooperative Research Center at Purdue University, is gratefully acknowledged.

Nomenclature

A_{cs} = cross-sectional area of a microchannel, mm^2
A_f = wetted area of a fin ($2Ld$), m^2
A_t = total heated area of all microchannels in a heat sink, m^2
Bl = boiling number, $Bl = q''_w/(Gh_{fg})$
Bo = bond number, $Bo = g(\rho_f - \rho_g)D^2/\sigma$
d = microchannel depth, μm
D = length scale ($\sqrt{A_{cs}}$), m
D_h = hydraulic diameter, μm
g = gravitational acceleration
G = mass flux, kg m^{-2} s^{-1}
h = heat transfer coefficient, W m^{-2} K^{-1}
h_{fg} = latent heat of vaporization for FC-77, J kg^{-1}
k_{si} = thermal conductivity of silicon, W/m K
L = microchannel length, m
N = number of microchannels in a test piece
$\dot{q}_{net}$ = heat dissipated to the fluid, W
q''_w = wall heat flux, W m^{-2}
Re = Reynolds number, $Re = GD/\mu$
T = temperature, °C
T_{ref} = reference temperature: T_f in single-phase region and T_{sat} in two-phase region, °C

w = microchannel width, μm
w_f = fin width, m

Greek Symbols

Δp = pressure drop, kPa
ρ = density, kg m^{-3}
η_o = overall surface efficiency of the microchannel heat sink
η_f = efficiency of a fin with an adiabatic tip, $\eta_f = \tanh md/md$ with $m^2 = 2h/(k_{si}w_f)$
μ = dynamic viscosity, kg m^{-1} s^{-1}
σ = surface tension, N m^{-1}

Subscripts

f = liquid
g = vapor
sat = saturated liquid
w = microchannel wall

References

[1] Garimella, S. V., and Sobhan, C. B., 2003, "Transport in Microchannels—A Critical Review," Ann. Rev. Heat Transfer, **13**, pp. 1–50.
[2] Sobhan, C. B., and Garimella, S. V., 2001, "A Comparative Analysis of Studies on Heat Transfer and Fluid Flow in Microchannels," Nanoscale Microscale Thermophys. Eng., **5**, pp. 293–311.f
[3] Bertsch, S. S., Groll, E. A., and Garimella, S. V., 2008, "Review and Comparative Analysis of Studies on Saturated Flow Boiling in Small Channels," Nanoscale Microscale Thermophys. Eng., **12**, pp. 187–227.
[4] Bertsch, S. S., Groll, E. A., and Garimella, S. V., 2009, "A Composite Heat Transfer Correlation for Saturated Flow Boiling in Small Channels," Int. J. Heat Mass Transfer, **52**, pp. 2110–2118.
[5] Bertsch, S. S., Groll, E. A., and Garimella, S. V., 2008, "Refrigerant Flow Boiling Heat Transfer in Parallel Microchannels as a Function of Local Vapor Quality," Int. J. Heat Mass Transfer, **51**, pp. 4775–4787.
[6] Bertsch, S. S., Groll, E. A., and Garimella, S. V., 2009, "Effects of Heat Flux, Mass Flux, Vapor Quality, and Saturation Temperature on Flow Boiling Heat Transfer in Microchannels," Int. J. Multiphase Flow, **35**, pp. 142–154.
[7] Liu, D., and Garimella, S. V., 2007, "Flow Boiling Heat Transfer in Microchannels," ASME J. Heat Transfer, **129**(10), pp. 1321–1332.
[8] Lee, P. S., and Garimella, S. V., 2008, "Saturated Flow Boiling Heat Transfer and Pressure Drop in Silicon Microchannel Arrays," Int. J. Heat Mass Transfer, **51**, pp. 789–806.
[9] Harirchian, T., and Garimella, S. V., 2008, "Microchannel Size Effects on Local Flow Boiling Heat Transfer to a Dielectric Fluid," Int. J. Heat Mass Transfer, **51**, pp. 3724–3735.
[10] Chen, T., and Garimella, S. V., 2006, "Effect of Dissolved Air on Subcooled Flow Boiling of a Dielectric Coolant in a Microchannel Heat Sink," ASME J. Electron. Packag., **128**(4), pp. 398–404.
[11] Harirchian, T., and Garimella, S. V., 2009, "The Critical Role of Channel Cross-Sectional Area in Microchannel Flow Boiling Heat Transfer," Int. J. Multiphase Flow, **35**, pp. 904–913.
[12] Harirchian, T., and Garimella, S. V., 2009, "Effects of Channel Dimension, Heat Flux, and Mass Flux on Flow Boiling Regimes in Microchannels," Int. J. Multiphase Flow, **35**, pp. 349–362.
[13] Jones, B. J., McHale, J. P., and Garimella, S. V., 2009, "The Influence of Surface Roughness on Nucleate Pool Boiling Heat Transfer," ASME J. Heat Transfer, **131**, p. 121009.
[14] Harirchian, T., and Garimella, S. V., 2010, "A Comprehensive Flow Regime Map for Microchannel Flow Boiling With Quantitative Transition Criteria," Int. J. Heat Mass Transfer, **53**, pp. 2694–2702.
[15] Chen, T., and Garimella, S. V., 2006, "Measurements and High-Speed Visualization of Flow Boiling of a Dielectric Fluid in a Silicon Microchannel Heat Sink," Int. J. Multiphase Flow, **32**(8), pp. 957–971.
[16] Chen, T., and Garimella, S. V., 2007, "Flow Boiling Heat Transfer to a Dielectric Coolant in a Microchannel Heat Sink," IEEE Trans. Compon. Packag. Technol., **30**(1), pp. 24–31.
[17] Jones, B. J., and Garimella, S. V., 2009, "Surface Roughness Effects on Flow Boiling in Microchannels," Proceedings of the ASME InterPACK '09, San Francisco, CA, Jul. 19–23.
[18] MATLAB, www.mathworks.com
[19] Harirchian, T., 2010, "Two-Phase Flow and Heat Transfer in Microchannels," Ph.D. thesis, Purdue University, West Lafayette, IN.
[20] Taylor, J. R., 1997, *An Introduction to Error Analysis*, 2nd ed., University Science Books, Sausalito, CA.
[21] Liu, D., and Garimella, S. V., 2004, "Investigation of Liquid Flow in Microchannels," J. Thermophys. Heat Transfer, **18**(1), pp. 65–72.
[22] Lee, P. S., Garimella, S. V., and Liu, D., 2005, "Investigation of Heat Transfer in Rectangular Microchannels," Int. J. Heat Mass Transfer, **48**, pp. 1688–1704.
[23] Holcomb, B. T., Harirchian, T., and Garimella, S. V., 2009, "An Experimental Investigation of Microchannel Size Effects on Flow Boiling With De-Ionized Water," Proceedings of the ASME Summer Heat Transfer Conference, HT2009, San Francisco, CA, Jul. 19–23.
[24] Harirchian, T., and Garimella, S. V., 2007, "Microchannel Size Effects on Two-Phase Local Heat Transfer and Pressure Drop in Silicon Microchannel Heat Sinks With a Dielectric Fluid," Proceedings of the ASME International Mechanical Engineering Congress and Exposition, IMECE2007, Vol. 11, Pt. A, pp. 437–446.
[25] Zhang, H. Y., Pinjala, D., and Wong, T. N., 2005, "Experimental Characterization of Flow Boiling Heat Dissipation in a Microchannel Heat Sink With Different Orientations," Proceedings of the Seventh Electronics Packaging Technology Conference, EPTC 2, pp. 670–676.
[26] Jiang, L., Wong, M., and Zohar, Y., 2001, "Forced Convection Boiling in a Microchannel Heat Sink," J. Microelectromech. Syst., **10**, pp. 80–87.
[27] Geisler, K. J. L., and Bar-Cohen, A., 2009, "Confinement Effects on Nucleate Boiling and Critical Heat Flux in Buoyancy-Driven Microchannels," Int. J. Heat Mass Transfer, **52**(11–12), pp. 2427–2436.
[28] Warrier, G. R., Dhir, V. K., and Momoda, L. A., 2002, "Heat Transfer and Pressure Drop in Narrow Rectangular Channels," Exp. Therm. Fluid Sci., **26**, pp. 53–64.
[29] Pate, D. P., Jones, R. J., and Bhavnani, S. H., 2006, "Cavity-Induced Two-Phase Heat Transfer in Silicon Microchannels," Proceedings of the Intersociety Conference on Thermal and Thermomechanical Phenomena and Emerging Technologies in Electronic Systems, pp. 71–78.
[30] Harirchian, T., and Garimella, S. V., "Flow Regime-Based Modeling of Heat Transfer and Pressure Drop in Microchannel Flow Boiling," Int. J. Multiphase Flow, in review.
[31] Cooper, M. G., 1984, "Heat Flow Rates in Saturated Nucleate Pool Boiling—A Wide-Ranging Examination Using Reduced Properties," Adv. Heat Transfer, **16**, pp. 157–239.
[32] Gorenflo, D., 1993, *VDI Heat Atlas*, VDI-Verlag, Dusseldorf, Chap. Ha.
[33] Chen, J. C., 1966, "Correlation for Boiling Heat Transfer to Saturated Fluids in Convective Flow," Ind. Eng. Chem. Process Des. Dev., **5**(3), pp. 322–329.
[34] Shah, M. M., 1977, "General Correlation for Heat Transfer During Subcooled Boiling in Pipes and Annuli," ASHRAE Trans., **83**(1), pp. 202–217.
[35] Gungor, K. E., and Winterton, R. H. S., 1986, "General Correlation for Flow Boiling in Tubes and Annuli," Int. J. Heat Mass Transfer, **29**(3), pp. 351–358.
[36] Tran, T. N., Wambsganss, M. W., and France, D. M., 1996, "Small Circular- and Rectangular-Channel Boiling With Two Refrigerants," Int. J. Multiphase Flow, **22**(3), pp. 485–498.
[37] Zhang, W., Hibiki, T., and Mishima, K., 2004, "Correlation for Flow Boiling Heat Transfer in Mini-Channels," Int. J. Heat Mass Transfer, **47**(26), pp. 5749–5763.
[38] Peters, J. V. S., and Kandlikar, S. G., 2007, "Further Evaluation of a Flow Boiling Correlation for Microchannels and Minichannels," Proceedings of the Fifth International Conference on Nanochannels, Microchannels and Minichannels, ICNMM2007, Puebla, Mexico, June 18–20.
[39] Baker, O., 1954, "Design of Pipe Lines for Simultaneous Flow of Oil and Gas," Oil & Gas J., **53**, pp. 185–195.
[40] Hewitt, G. F., and Robert, D. N., 1969, "Studies of Two-Phase Flow Patterns by Simultaneous X-Ray and Flash Photography," HMSO, Report No. AERE-M 2159.
[41] Taitel, Y., and Dukler, A. E., 1976, "A Model for Predicting Flow Regime Transitions in Horizontal and Near Horizontal Gas-Liquid Flow," AIChE J., **22**, pp. 47–55.
[42] Hetsroni, G., Mosyak, A., Segal, Z., and Pogrebnyak, E., 2003, "Two-Phase Flow Patterns in Parallel Microchannels," Int. J. Multiphase Flow, **29**, pp. 341–360.
[43] Huo, X., Chen, L., Tian, Y. S., and Karayiannis, T. G., 2004, "Flow Boiling and Flow Regimes in Small Diameter Tubes," Appl. Therm. Eng., **24**, pp. 1225–1239.
[44] Revellin, R., Dupont, V., Ursenbacher, T., Thome, J. R., and Zun, I., 2006, "Characterization of Diabatic Two-Phase Flows in Microchannels: Flow Parameter Results for R-134a in a 0.5 mm Channel," Int. J. Multiphase Flow, **32**, pp. 755–774.
[45] Chung, P. M.-Y., and Kawaji, M., 2004, "The Effect of Channel Diameter on Adiabatic Two-Phase Flow Characteristics in Microchannels," Int. J. Multiphase Flow, **30**(7–8), pp. 735–761.
[46] Hassan, I., Vaillancourt, M., and Pehlivan, K., 2005, "Two-Phase Flow Regime Transitions in Microchannels: A Comparative Experimental Study," Nanoscale Microscale Thermophys. Eng., **9**, pp. 165–182.
[47] Field, B., and Hrnjak, P., 2007, "Visualization of Two-Phase Refrigerant and Refrigerant-Oil Flow in a Microchannel," ASME International Mechanical Engineering Congress and Exposition, Seattle, WA, Paper No. IMECE2007-43471.